

Balancing Accuracy, Delay and Battery Autonomy for Pervasive Seizure Detection

Athanasios Karapatis^{1,2,†}, Robert M. Seepers^{1,†}, Marijn van Dongen², Wouter A. Serdijn², Christos Strydis^{1,†}

¹Dept. of Neuroscience, Erasmus Medical Center, Rotterdam, The Netherlands

²Section Bio-electronics, Delft University of Technology, The Netherlands

Corresponding authors: {r.seepers, c.strydis}@erasmusmc.nl

Abstract—A promising alternative for treating absence seizures has emerged through closed-loop neurostimulation, which utilizes a wearable or implantable device to detect and subsequently suppress epileptic seizures. Such devices should detect seizures fast and with high accuracy, while respecting the strict energy budget on which they operate. Previous work has overlooked one or more of these requirements, resulting in solutions which are not suitable for continuous closed-loop stimulation. In this paper, we perform an in-depth design space exploration of a novel seizure-detection algorithm, which uses a complex Morlet wavelet filter and a static thresholding mechanism to detect absence seizures. We consider both the accuracy and speed of our detection algorithm, as well as various trade-offs with device autonomy when executed on a low-power processor. For example, we demonstrate that a minimal decrease in average detection rate of only 1.83% (from 92.72% to 90.89%) allows for a substantial increase in device autonomy (of 3.7x) while also facilitating faster detection (from 710 ms to 540 ms).

I. INTRODUCTION

Absence epilepsy is a neurological disease characterized by episodes of transient impairment of consciousness (called seizures or ictal events). In spite of a number of available treatments (i.e. medication and surgery), absence epilepsy is yet to be treated effectively. However, several studies have shown the potential of closed-loop neurostimulation for the treatment of epileptic seizures [2], [4], [5], [8], [12]. These systems monitor brain activity using Electroencephalography (EEG) or Electrocorticography (ECoG) and suppress seizure manifestation by applying electrical or optical neurostimulation upon detection.

In practice, a closed-loop stimulator would be realized as a wearable (or implantable) device for providing continuous and mobile treatment. To maximize treatment efficacy, such devices should detect seizures both accurately and fast, allowing seizures to be suppressed prior to significant manifestation. Furthermore, these devices typically operate autonomously (i.e., they are battery powered), putting severe restrictions on its energy consumption. However, existing studies have not considered all these requirements and have instead focused (primarily) on either fast, accurate or lightweight detection algorithms [3], [7], [9], resulting in

algorithms that are not suitable for continuous closed-loop stimulation.

In this work, we evaluate the suitability of a novel seizure-detection algorithm for the treatment of absence epilepsy, based on a complex Morlet wavelet and a static thresholding mechanism. A preliminary evaluation of the algorithm has shown promising results in terms of both its detection accuracy and detection delay [12]. Moreover, the (computational) simplicity of the algorithm makes it a potential candidate for wearable or implantable devices. We consider the effects of various algorithmic parameters on its detection performance and energy consumption, including the number and offset of filter coefficients and different threshold levels. To the best of our knowledge, this is the first work which considers all design goals relevant to continuous closed-loop stimulation and describes various trade-offs between them.

The remainder of this paper is structured as follows: First, we discuss studies related to seizure detection in Section II. The complex Morlet wavelet and its application in the seizure-detection system is described in Section III and subsequently evaluated in Section IV. Finally, concluding remarks are provided in Section V.

II. RELATED WORK

Absence and generalized seizures exhibit increased oscillatory neural activity in the brain [5], which has made frequency-based filtering (e.g., using wavelets) a prime candidate for detection. In this Section, we first describe studies which focus on detecting epileptic events accurately and/or fast, after which we discuss low-power implementations.

One of the first studies using wavelets presents a seizure-detection algorithm using a level-3 DAUB4 wavelet along with a median filter [7]. The proposed solution achieves an average detection delay of 3.3 s, with a perfect true-positive rate (i.e., rate of correctly detecting seizures) of 100% and a low False-Positive-per-seizure rate of 0.04. A combination of wavelet-based input filtering and an Artificial Neural Network was proposed in [1]. After considering various wavelets, a maximum average detection rate (ADR) of 95.8% is obtained using a Biorthogonal (bior1.3, bior1.5) wavelet. In [3], a combination of a level-3 DAUB4 wavelet and reservoir computing is proposed as a classification method, demonstrating that seizures may be detected both fast (in

[†]This work was supported by the H2020 ICT-32-2014 project SHARCS under Grant Agreement No. 644571 and would not have been complete without the invaluable support of Dr. F.E. Hoebeek.

0.97 sec) and accurately (ADR of 97.2%). While these solutions are capable of detecting seizures accurately and at minimal delay, they employ computationally expensive algorithms, making them unsuitable for wearable or implantable devices.

Given the limited energy budget, several low power ASIC implementations have been proposed to form minimalistic detection methods. For example, it is proposed in [6] to use a Daubencies-4 wavelet and thresholding for classification, resulting in an ADR of 97% and an average power consumption of 440 μ W. Another study proposes to exploit the increase in oscillatory neural activity using a simple thresholding mechanism in the frequency domain [10]. This results in minimal power consumption (50 μ W) and a perfect true-positive rate of 100%, yet results in a high detection delay of 13.5 s. An ultra-lightweight solution is proposed in [9], where thresholding is applied on the amplitude on the raw EEG signal (time domain). The simplicity of this solution has a substantial (negative) impact on the ADR (92.1%), yet sports an ultra-low power consumption of under 350 nW and a detection delay of 8.5 s. We note that these low-power implementations exhibit a high detection delay, making them ineffective for closed-loop stimulation.

III. SYSTEM DESCRIPTION

In this Section, we describe the complex Morlet wavelet filter and how it is applied for seizure detection. Previous work has shown that this wavelet is well-suited for the detection of Spike-Wave Discharges (SWDs, a hallmark feature of absence seizures [5]), given their morphology. A practical FIR implementation of this filter defines the filter output as the total power of its real and imaginary components [12]; that is:

$$P_{FIR} = \left(\sum_{i=0}^{N-1} Re[c_i]x[n-i] \right)^2 + \left(\sum_{i=0}^{N-1} Im[c_i]x[n-i] \right)^2 \quad (1)$$

where P_{FIR} is the filter output, x are the input samples, N is the order of the filter and c_i are the filter coefficients. As a baseline, we designed an FIR filter which closely approximates the ideal Morlet wavelet with $N = 229$ coefficients using the effective support range for the wavelet as provided by the MATLAB Wavelet Toolbox, the impulse response of which is depicted in Figure 1.

Let us now consider the use of the Morlet wavelet in seizure detection, exemplified in Figure 2 and showing ECoG input (top) and the corresponding filter output (bottom). As depicted, the average filter response during ictal events is expectedly higher compared to inter-ictal periods: This allows us to identify ictal events in the input signal using a simple thresholding mechanism, where a seizure is detected when an upper threshold ($V_{th,h}$) is crossed. Upon detection, a closed-loop system would start stimulating brain tissue until the seizure is suppressed, detected using a lower threshold $V_{th,l}$ that is set to the average filter output during inter-

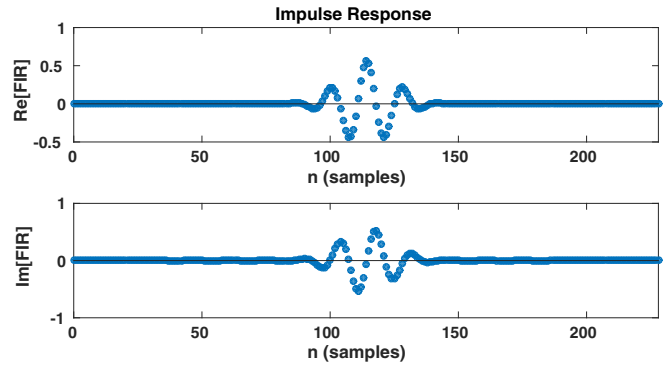


Fig. 1: Impulse response for the baseline complex Morlet-wavelet filter, consisting of 229 coefficients.

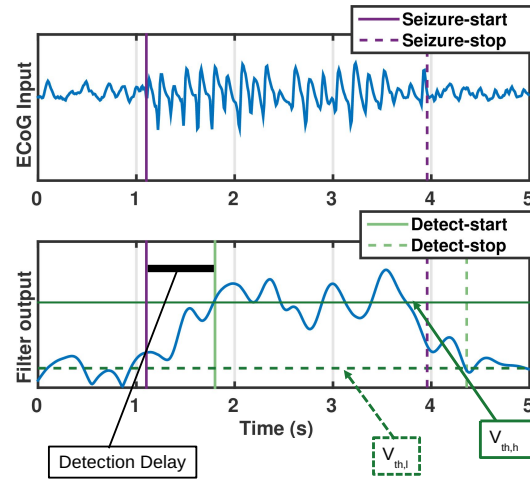


Fig. 2: SWD-detection using the Morlet wavelet filter. Top: ECoG recordings where a seizure occurs between the "Start" and "Stop" annotations. Bottom: Filter output P_{FIR} , where a seizure is detected after some delay.

ictal periods¹. Finally, Figure 2 reveals that a delay occurs between the onset of a seizure and detection. Both this delay and the seizure-detecting capabilities are a direct function of the filter implementation and $V_{th,h}$, as discussed in the following section.

IV. EVALUATION

To explore the various trade-offs between seizure-detection accuracy, delay and device autonomy, we next evaluate various instances of our detection algorithm. First, we introduce our experimental setup in Section IV-A, after which the algorithm is evaluated in Section IV-B.

A. Experimental Setup

We start by presenting our figures of merit, after which we continue by describing the detection-algorithm parameters and conclude with the datasets used in our evaluation.

¹Note that $V_{th,l}$ is used to identify seizure suppression and has no direct influence on the algorithm's detection capabilities.

1) *Evaluation metrics*: The algorithm is evaluated in terms of detection accuracy, detection delay and device autonomy (energy consumption). The average detection rate (ADR) quantifies how accurately inter-ictal periods (i.e., periods without seizures) are distinguished from ictal events (seizures) and is defined as $ADR = \frac{TPR + TNR}{2}$, where TPR is the true positive rate (also known as sensitivity) and TNR is the true negative rate (also known as specificity). TPR signifies the percentage of correctly classified seizures and is defined as $TPR = \frac{TP}{(FN+TP)}$, where TP = true positive (correct detection of a seizure) and FN = false negative (absence of detection during a seizure). A high TPR indicates that the filter detects most seizures correctly, which would allow a closed-loop stimulator to identify and suppress most seizures. Analogously, TNR specifies how well inter-ictal periods are correctly classified, that is, $TNR = \frac{TN}{(FP+TN)}$, where TN = true negative (correct detection of an inter-ictal period) and FP = false positive (incorrect seizure indication). A high TNR means that few inter-ictal events are falsely classified as seizures, minimizing the adverse effects experienced by a patient resulting from undesired stimulation.

The detection delay T_d is the time between the onset of an ictal event and the time at which it is detected by the filter. A low detection T_d is beneficial as it allows for seizure suppression prior to significant manifestation.

To evaluate device autonomy, the detection algorithm is executed on the low-power SiMS processor [11]. To get an accurate estimation of autonomy, we first synthesize the SiMS processor for a UMC 90nm CMOS technology in Synopsys Design Compiler using Faraday SP libraries (due to availability). We subsequently obtain the switching activity of the algorithm executed on the SiMS processor using RTL simulation in ModelSim. An estimation of the energy consumption is subsequently obtained by evaluating the switching activity for the synthesized core in Synopsys PrimeTime. Finally, autonomy is derived by normalizing this energy consumption to a reference battery capacity of 0.1 mWh. A high autonomy allows the device to stay on for a prolonged period of time, benefiting its operational lifetime.

2) *Detection parameters*: The baseline filter accurately approximates a continuous complex Morlet wavelet using $N = 229$ coefficients. To trade-off detection performance and autonomy, we evaluate various instances of this filter using a subset of these coefficients (the "coefficient window"), as illustrated in Figure 3. This coefficient window has two parameters which are varied in our evaluation: 1) The window size, i.e., the number of coefficients N selected in the subset. Decreasing N results in a less accurate approximation of the ideal Morlet wavelet, which expectedly decreases both detection accuracy and computational overheads; and 2) The window offset: The default filter is symmetric (offset = 0), in which the most significant component of the impulse response revolves around the center coefficients of the filter. By shifting the window to the left (-) or right (+) from the impulse response center, we attempt to obtain more favorable detection properties by having this significant component

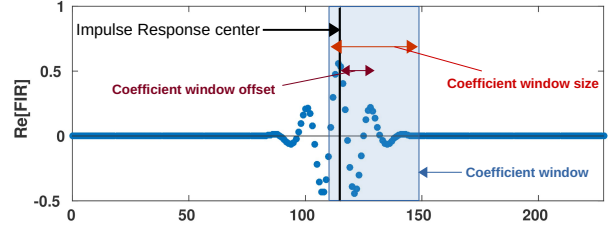


Fig. 3: Coefficient window (depicted for the real part of the impulse response).

appear earlier or later in the selected coefficients.

In addition, the filter performance is a function of the upper threshold $V_{th,h}$. As illustrated in Figure 2, a low $V_{th,h}$ minimizes the filter output required for seizure detection, allowing ictal events to be detected accurately and fast at the cost of increased FPs . Conversely, a high $V_{th,h}$ may decrease the number of FPs , while also lowering the number of ictal events correct classified as such. To quantify the filter performance as a function of $V_{th,h}$, we vary it between $V_{th,h}^{min} \leq V_{th,h} \leq V_{th,h}^{max}$ (in 64 uniformly distributed steps), where $V_{th,h}^{min}$ ($V_{th,h} = 1$) and $V_{th,h}^{max}$ ($V_{th,h} = 64$) are the thresholds at which ictal events are detected with 100% and 70% accuracy, respectively. Note that $V_{th,h}^{min}$ and $V_{th,h}^{max}$ are chosen to be relative to the filter output: This allows for a fairer comparison between different filters, which are known to exhibit different output amplitudes.

3) *Dataset*: For our evaluation, we have considered a dataset consisting of 29.75 hours (split in traces of 15 minutes) of prerecorded ECoG data from 24 subjects (mice), obtained using a Digidata 1322A digitizer and a CyberAmp amplifier (Molecular Devices, Axon Instruments, Sunnyvale, CA). The data was annotated to determine time stamps at which seizures start and end, where a seizure was defined as (at least) 500 ms of SWD activity with a repetition rate of at least 5 Hz [3], [5], [12]. The time stamps were obtained using an in-house, off-line algorithm that uses peak detection and validated visually by an experienced neuroscientist. The dataset contains a total of 1914 seizures.

B. Experimental Results

In this Section, we evaluate various trade-offs between detection performance and device autonomy (energy expenditure) for our algorithm. Our evaluation is structured as follows: First, we describe the detection performance for a symmetric filter (offset = 0), after which we consider the effect of asymmetric filtering. We subsequently describe various pseudo-optimal filter settings (Pareto points), followed by a comparison between detection performance and device autonomy. Finally, we briefly compare our obtained results to those reported in related work.

1) *Detection performance*: To understand the effects of different window sizes N and thresholds $V_{th,h}$ on the detection performance, we first restrict ourselves to a symmetric filter (offset = 0). The resulting TPR, TNR, ADR and T_d are depicted in Figure 4 for three different threshold levels ($V_{th,h} = 25, 44, 64$, i.e., relatively low, average and high threshold)

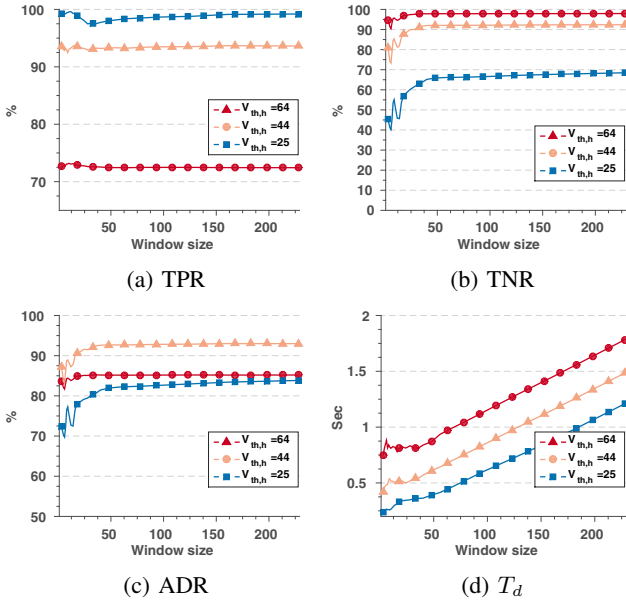


Fig. 4: Detection performance for a symmetric filter (offset=0) as a function of the number of coefficients N and various thresholds.

and are next discussed in-order. Recall that $V_{th,h}^{max}$ and $V_{th,h}^{min}$ are chosen relative to filter output and detected ictal events (TPs). As TPR is a direct function of the percentage of TPs (and FNs), we find no change as a function of N for a given $V_{th,h}$. Different thresholds, however, have a more profound effect on TPR, i.e., increasing $V_{th,h}$ results in decreased TPR.

Contrary to TPR, we find that TNR (Figure 4 (b)) is substantially affected by both N and $V_{th,h}$ and increasing either parameter results in increased TNR. This is explained as follows: First, the filter more accurately approximates the ideal Morlet wavelet for larger N , resulting in a larger difference in filter output between ictal events and inter-ictal periods and, accordingly, a more accurate classification for a given $V_{th,h}$. Second, increasing $V_{th,h}$ requires a higher filter output for an inter-ictal period to be classified as a seizure, resulting in less FPs and more TNs and also increasing TNR. As ADR is the average of TPR and TNR and the former is relatively constant irrespective of N , ADR (Figure 4 (c)) follows the same trends as TNR.

Finally, Figure 4 (d) depicts T_d , which scales linearly as a function of N for a given $V_{th,h}$. We attribute this scaling to the symmetric nature of our filter, in which the significant components of the impulse response are found in the center coefficients of the filter. As a result, increasing N means that a larger history of samples is required before the input reaches this center point, leading to a delay in high filter output and, therefore, a slower detection for a given $V_{th,h}$. Conversely, lowering $V_{th,h}$ may speed up detection due to requiring a lower filter output.

The effect of N on T_d motivates us to investigate an asymmetric filter, in which the coefficient window is shifted by an offset. In doing so, the resulting filter effectively

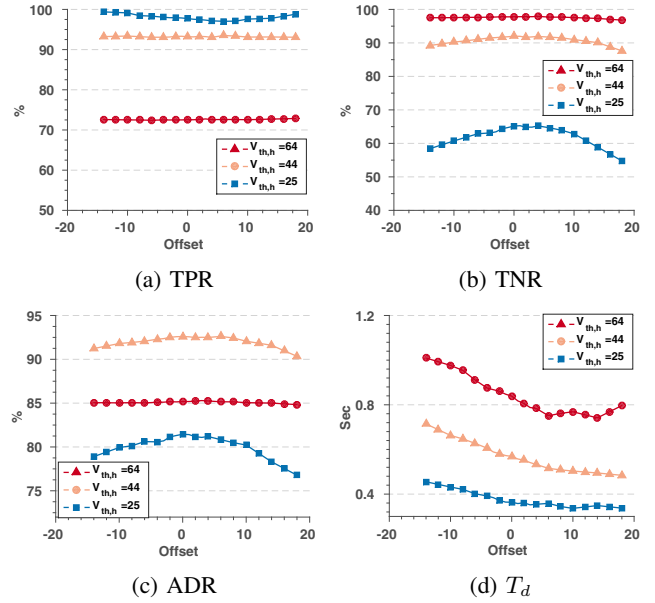


Fig. 5: Detection performance for an asymmetric filter ($N = 40$) as a function of coefficient-window offset and various thresholds.

deviates from a complex Morlet wavelet; however, we expect that this allows us to achieve a better T_d , while maintaining similar detection accuracies. Figure 5 presents the detection performance as a function of the offset with a fixed window size of $N = 40$ (other N show similar trends and are, therefore, not discussed in detail).

As expected, we find that detection accuracy (TPR, TNR, ADR) is not substantially affected by various offset values, attributed to maintaining the significant coefficients as part of the coefficient window. T_d (Figure 5d), however, is increased when the coefficient window is shifted left (-offset) and decreased by shifting to the right (+offset). That is, by moving the significant peak of filter coefficients to earlier in the coefficient window, we minimize T_d while maintaining similar accuracy.

Up until this point, we have described the effect of the various algorithmic parameters (N , $V_{th,h}$ and offset) have on the seizure-detecting performance. That is, increasing N increases TNR, ADR and T_d ; increasing $V_{th,h}$ leads to decreased TPR and T_d and increased TNR and ADR; and a positive filter offset shows a decrease in T_d . Now understanding these input-output relations, we exhaustively evaluate all possible filter instances in order to derive a set of Pareto points (i.e., solutions which are Pareto optimal).

The resulting Pareto front is depicted in Figure 6, where different coefficient-window sizes (N) are highlighted to illustrate the various trends in each output value. Briefly stated, we find a positive correlation between TPR and T_d , i.e., an increase in TPR results in a decrease in T_d for a given N . As TPR does not vary with N , this means that we can get a ‘free’ improvement in T_d by choosing smaller N . A similar trend is observed in Figure 6 (c), i.e., reducing N

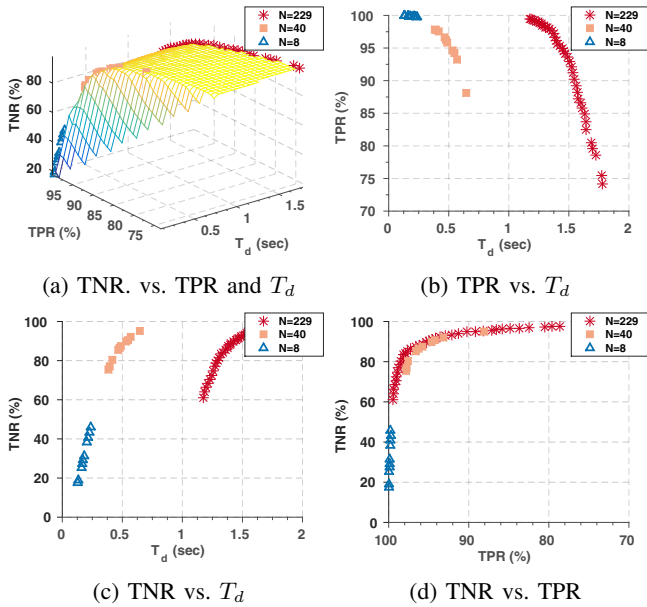


Fig. 6: Pareto front for TPR, TNR, and T_d . High-lighted are points that correspond to various window sizes ($N=8,40,229$).

allows us to obtain a similar TNR with reduced T_d . Finally, Figure 6 (d) depicts the counteractive behavior between TPR and TNR, i.e., a high TPR leads to a low TNR and vice versa, attributed to the way in which they respond to different $V_{th,h}$.

2) *Device autonomy*: In the previous subsection, we have performed an in-depth study of the detection accuracy and delay. However, as our algorithm is intended for wearable or implantable devices, it has to consume minimal energy to ensure device autonomy. We next describe the trade-offs between filter performance and device autonomy, assuming a reference battery capacity of 0.1 mWh.

Figure 7 depicts the battery lifetime (in weeks) as measured on the SiMS processor, as well as ADR and detection delay. For simplicity, we restrict our evaluation here to filters with maximum ADR for a given N (other filter-settings show similar trends and are therefore not discussed in detail). Note that the battery lifetime only varies with N as it defines the number of arithmetic operations performed (see Eq. 1). Logically, this means that the battery lifetime is reduced when N is increased.

Starting from $N = 7$, we find a low ADR (86.83%) and detection delay (of 0.58 seconds), with a large battery lifetime (11.8 weeks). Increasing the window size favors detection accuracy, yet increases both detection delay and execution time (and in turn energy expenditure). As a result, increasing N shows a (slight) improvement in ADR, up to a maximum of roughly 92.27% ($N = 70$), yet diminishes battery lifetime substantially (down to 1.18 weeks for the same $N = 70$). Effectively, in order to increase detection accuracy we require a better filter approximation which can be achieved by using a larger window size at the cost of device autonomy. Conversely, in order to increase

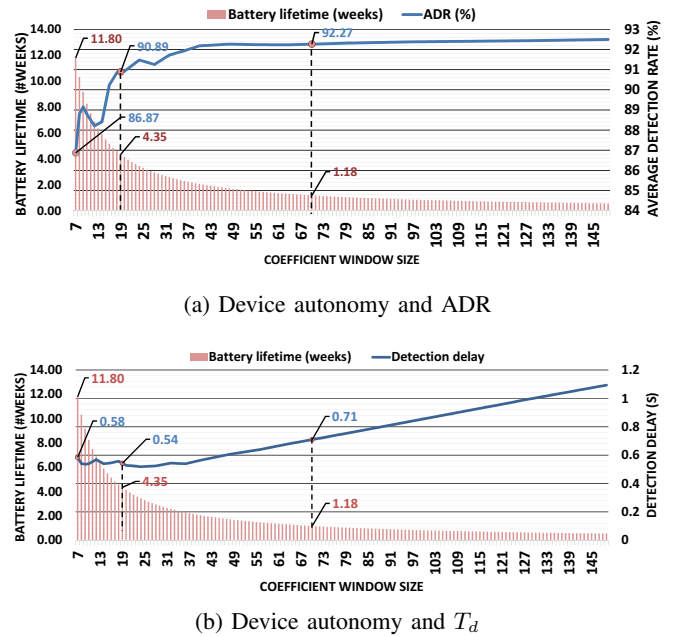


Fig. 7: Device autonomy, ADR and T_d as a function of the number of filter coefficients.

battery lifetime we need low computational overheads which are obtained by using less filter coefficients. The results demonstrate that a careful trade-off can substantially benefit device autonomy: For example, lowering the ADR by only 1.38% (to 90.89% for $N=19$), allows for an extension of device autonomy by 3.7x (up to 4.4 weeks). Furthermore, this decrease in N reduced detection delay by 0.17 seconds (to 540 ms).

3) *Comparison to related work*: We can now compare our algorithm to related works, the results of which are presented in Table I. Here, we have chosen to compare the design point with improved device autonomy (of 4.4 weeks) described in the previous subsection. While not all related works report on all design goals relevant to closed-loop stimulation, the results in Table I suggest that algorithms based on the complex Morlet wavelet (this work and [12]) may detect seizures considerably faster, albeit with a slight reduction in ADR. Of course, it is possible to increase the ADR if desired (at the cost of detection delay) by fine-tuning the algorithm's parameters.

Table I furthermore depicts the power consumption of our and other lightweight implementations. Unfortunately, these results can not be compared directly: Our evaluation has considered the detection algorithm in isolation and has excluded other components which are normally part of a closed-loop system, such as circuits for signal conditioning, analog/digital conversion and packaging effects. In contrast, related work has included these components, producing a higher (and more accurate) estimation of the power consumption. On the other hand, our algorithm has been implemented in software and is executed on a generic processor. This has allowed us to rapidly explore the effect of the input

TABLE I: Comparison of the performance of various seizure-detection systems.

Reference	[1]	[6]	[10]	[9]	[7]	[3]	[12]	This Work**
Detection delay (s)	unknown	unknown	13.5	8.5	3.3	0.97	0.50	0.54
Average detection rate	0.96	0.97	unknown	0.92	0.96	0.97	0.95	0.91
Power consumption (μ W)	unknown*	440	50	0.4	unknown	unknown*	unknown	0.107

*: Expected to have a high power consumption.

**: Only detection algorithm considered in evaluation.

parameters on our design goals; however, this approach is known to be substantially less efficient than custom hardware designs (employed in related work). In future work, we intend to both provide a custom hardware implementation and evaluate our algorithm in a more realistic closed-loop setting.

V. CONCLUSION

In this paper we have performed a design-space exploration into a novel and flexible seizure-detection algorithm, which uses a complex Morlet wavelet filter and a static thresholding mechanism. The algorithm has been evaluated in terms of detection performance (true-positive rate, true-negative rate, average-detection rate and detection delay) and device (battery) autonomy, considering a variety of algorithmic parameters (threshold levels and the number and offset of filter coefficients). It has been shown that non-trivial trade-offs can be made between various aspects of detection performance and energy overheads. For example, a minimal decrease in average-detection rate of 1.38% (from 92.27% to 90.89%) allows for an increasing device autonomy by 3.7x, while promoting faster detection (from 710 ms to 540 ms). Our work demonstrates that future seizure-detection algorithms for closed-loop stimulation should be carefully adapted to its intended use, so as to both maximize its detection performance and energy efficiency.

REFERENCES

- [1] A. Berdakh and S. H. Don. Epileptic seizures detection using continuous time wavelet based artificial neural networks. In *Information Technology: New Generations, 2009. ITNG'09. Sixth International Conference on*, pages 1456–1461. IEEE, 2009.
- [2] A. Berényi, M. Belluscio, D. Mao, and G. Buzsáki. Closed-loop control of epilepsy by transcranial electrical stimulation. *Science*, 337(6095):735–737, 2012.
- [3] P. Buteneers, D. Verstraeten, B. Van Nieuwenhuysse, D. Stroobandt, R. Raedt, K. Vonck, P. Boon, and B. Schrauwen. Real-time detection of epileptic seizures in animal models using reservoir computing. *Epilepsy research*, 103(2):124–134, 2013.
- [4] E. E. Fanselow, A. P. Reid, and M. A. Nicolelis. Reduction of pentylentetrazole-induced seizure activity in awake rats by seizure-triggered trigeminal nerve stimulation. *The Journal of Neuroscience*, 20(21):8160–8168, 2000.
- [5] L. Kros, O. H. Eelkman Rooda, J. K. Spanke, P. Alva, M. N. Dongen, A. Karapatis, E. A. Tolner, C. Strydis, N. Davey, B. H. Winkelman, et al. Cerebellar output controls generalized spike-and-wave discharge occurrence. *Annals of neurology*, 77(6):1027–1049, 2015.
- [6] H. Markandeya, G. Karakonstantis, S. Raghunathan, P. Irazoqui, and K. Roy. Low-power dwt-based quasi-averaging algorithm and architecture for epileptic seizure detection. In *Proceedings of the 16th ACM/IEEE international symposium on Low power electronics and design*, pages 301–306. ACM, 2010.
- [7] I. Osorio, M. G. Frei, and S. B. Wilkinson. Real-time automated detection and quantitative analysis of seizures and short-term prediction of clinical onset. *Epilepsia*, 39(6):615–627, 1998.
- [8] J. T. Paz, T. J. Davidson, E. S. Frechette, B. Delord, I. Parada, K. Peng, K. Deisseroth, and J. R. Huguenard. Closed-loop optogenetic control of thalamus as a tool for interrupting seizures after cortical injury. *Nature neuroscience*, 16(1):64–70, 2013.
- [9] S. Raghunathan, S. K. Gupta, M. P. Ward, R. M. Worth, K. Roy, and P. P. Irazoqui. The design and hardware implementation of a low-power real-time seizure detection algorithm. *Journal of neural engineering*, 6(5):056005, 2009.
- [10] M. T. Salam, M. Sawan, and D. K. Nguyen. A novel low-power-implantable epileptic seizure-onset detector. *Biomedical Circuits and Systems, IEEE Transactions on*, 5(6):568–578, 2011.
- [11] C. Strydis et al. A system architecture, processor and communication protocol for secure implants. *TACO*, 2013.
- [12] M. N. van Dongen, A. Karapatis, L. Kros, O. Eelkman Rooda, R. M. Seepers, C. Strydis, C. De Zeeuw, F. Hoebeek, W. Serdijn, et al. An implementation of a wavelet-based seizure detection filter suitable for realtime closed-loop epileptic seizure suppression. In *Biomedical Circuits and Systems Conference (BioCAS), 2014 IEEE*, pages 504–507. IEEE, 2014.